Check for updates

ADVANCED INTELLIGENT SYSTEMS
Open Access
www.advintellsyst.com

Modular Stimuli-Responsive Valves for Pneumatic Soft Robots

*Qiguang He, Rui Yin, Yucong Hua, Hang Shu, Xiaoheng Zhu, A. B. M. Tahidul Haque, Samuele Ferracin, Saheli Patel, Weijian Jiao, and Jordan R. Raney**

Pneumatic soft robots have several advantages, including facile fabrication, versatile deformation modes, and safe human–machine interaction. However, pneumatic soft robots typically rely on mechatronics to interact with their environment, which can limit their form factors and reliability. Researchers have considered how to achieve autonomous behaviors using the principles of mechanical computing and physical intelligence. Herein, modular responsive valves that can autonomously regulate airflow within pneumatic soft robots in response to various environmental stimuli, including light, water, and mechanical forces, are described. By combining multiple types of valves, autonomous logic gates and more advanced logical operations can be realized. Finally, it is demonstrated that responsive valves can be integrated with pneumatic soft robots, allowing autonomous morphing and navigation. This framework provides a strategy for creating autonomous pneumatic robots that can respond to multiple stimuli in their environment.

1. Introduction

Pneumatic soft robots have been of growing interest over the last couple decades[1–3] for their potential advantages, including facile fabrication,[4] fast response,[5] compliance,[6,7] versatility of deformation modes,[8] resilience under harsh conditions,[9] and safe interaction with humans.[10–12] These promising features have enabled the design of robots with numerous advantages related to grasping,[5,7] manipulation,[13] morphing,[14] and locomotion.[4,15] However, it is still challenging to achieve autonomous behaviors in these systems. To sense and respond to the environment, conventional mechatronic devices are typically integrated with the pneumatic soft robots,[16–18] which can limit the form factor of the robots and may also constrain their reliability under harsh environments (e.g., environments with strong radiation or electromagnetic fields).

Recently, researchers have been considering how autonomy might be embodied in pneumatic soft robots using principles from mechanical computation and physical intelligence.[19–21] For example, to simplify the pneumatic control system, Rothemund et al. developed bistable valves that regulate airflow based on a snap-through instability.[22] Preston et al. built digital logic circuits and soft ring oscillators, enabling the soft robot to produce oscillatory movements in locomotion and manipulation.[23] Drotman et al. further integrated sensing in a soft-legged quadruped that autonomously reverses its moving direction once it contacts a physical object.[24] In all these examples, physical intelligence is achieved via structural design that enables the system to respond to mechanical forces. However, real-world scenarios may require that pneumatic robots sense and interact with additional stimuli,[4,25] such as temperature, humidity, and so on.

Previous work has begun to address this challenge by incorporating responsive materials in robotic designs. These materials enable autonomous behaviors in response to additional stimuli. Examples include liquid crystal elastomers (LCEs) that can respond to heat and light due to a nematic–isotropic phase transition,[26] shape-memory polymers (SMPs) that can change shape and stiffness under heat,[27] hydrogels that swell in the presence of water,[28] soft magnetic composites that actuate in the presence of magnetic fields,[29,30] and so on. Multiple types of responsive materials can be combined and distributed throughout the soft bodies of the pneumatic soft robots, allowing robots to autonomously adjust their behaviors and navigate through dynamic or uncertain environments based on stimuli-responsive modules that control the trajectory of the robot via multiple localized mechanical constraints.[31] However, this approach has only been used to enable limited autonomous trajectory changes, and it is difficult to see how mechanical constraints could be extended to more advanced autonomous functions. Thus, achieving a broader, more generalized set of autonomous behaviors in pneumatic soft robots remains a challenge, and will require new strategies.

Q. He, R. Yin, Y. Hua, H. Shu, X. Zhu, A. B. M. T. Haque, S. Ferracin, S. Patel, W. Jiao, J. R. Raney
Department of Mechanical Engineering and Applied Mechanics
University of Pennsylvania
Philadelphia, PA 19104, USA
E-mail: raney@seas.upenn.edu

Q. He
Department of Mechanical and Automation Engineering
The Chinese University of Hong Kong
Hong Kong SAR 999077, China

The ORCID identification number(s) for the author(s) of this article can be found under https://doi.org/10.1002/aisy.202400659.

© 2024 The Author(s). Advanced Intelligent Systems published by Wiley-VCH GmbH. This is an open access article under the terms of the Creative Commons Attribution License, which permits use, distribution and reproduction in any medium, provided the original work is properly cited.

DOI: 10.1002/aisy.202400659

In this work, building on recent advances in pneumatic valves, responsive materials, and embodiment, we demonstrate a strategy for designing modular responsive valves that autonomously regulate the flow of air in pneumatic soft robots in response to environmental stimuli. Convenient to manufacture and simple to use, these valves can be combined to achieve logic gates and more complex logical computation (**Figure 1** and S1, Supporting Information). The responsive valves consist of responsive materials, such as LCEs and hydrogels, combined with mechanisms that cause the actuation of the material to open or close pneumatic valves. When the responsive materials are exposed to relevant external stimuli, including light, moisture, and mechanical force, they actuate, squeezing or releasing a soft tube. In this way, the mechanism achieves basic logic by enabling or obstructing airflow. By connecting multiple responsive valves in series or in parallel, more complex logic networks can be created, which, in turn, control the morphology or motion of pneumatic soft robots.

2. Results

2.1. Design, Construction, and Operating Principle of Modular Responsive Valves

Each responsive valve is designed to sense and respond to particular external stimuli, which could include light, water, and mechanical force (Figure S1, Supporting Information). As shown in **Figure 2**, these responsive valves comprise responsive materials (Figure S2, Supporting Information), 3D-printed rigid parts (a piston, a chamber, a fixed end), a soft silicone tube, and a pair of magnets. As demonstrated in previous studies, carbon nanotube-doped LCE composites (CNT-LCEs) can generate large actuation strain when exposed to light (via the photothermal mechanism[32–35]); hydrogels (wrapped with a constraining braided mesh) can produce large stress and contraction when exposed to water.[36]

As shown in Figure 2A,B, these responsive materials can open or close air channels when subjected to relevant stimuli. The valve shown in Figure 2A is designed to be closed by default. A pair of magnets compresses the soft tube, preventing the passage of air until relevant stimuli (light, water) are applied to the valve, causing contraction of the responsive materials (CNT-LCE, hydrogel), lifting the piston, and opening the valve. The change of state of the valve is reversible; the responsive materials can fully recover to their initial shape, causing the return of the valve to its closed state (Figure 2A).

A minor redesign allows the construction of valves that are open by default, which close when relevant stimuli are introduced (Figure 2B). As above, the stimuli cause the materials to contract. However, a redesign of the mechanism causes this contraction to close the air channel when relevant stimuli are applied (Figure 2B). The removal of the stimuli returns the valve to its default open state, which is facilitated by the attraction of the pair of magnets. Of course, one can also design the valves to be switchable via mechanical force rather than using stimuli-responsive materials. Figure 2C,D shows designs for such valves, which are closed or open by default, respectively. It is worth noting that, while we focus here on valves that can change state reversibly, one can make valves that permanently change state simply by tuning the strength of the magnets. Figure S3, Supporting Information, shows an example of this behavior, which uses extra magnets to make the state change permanent.

2.2. Characterization of Responsive Valves

To characterize these responsive valves, we built a pressure control system with an air pump and solenoid valve controlled via pulse width modulation (PWM). This was connected to the valves and a pneumatic actuator as shown in **Figure 3**A. The shape of the pneumatic actuator shows the "ON" and "OFF" states of the responsive valve while external stimuli were applied to the valves. The values of input source pressure (P_1) and the pressure of the actuator (P_2) were measured simultaneously with two pressure sensors. Six different modules (Figure 3A) were used in this work, with different colors indicating different default states: 1) yellow valves are light-responsive and closed by default; 2) blue valves are water-responsive and closed by default; 3) green valves are mechanical valves and closed by default; 4) red valves are light-responsive and open by default; 5) white valves are water-responsive and open by default; and 6) gray valves are mechanical valves and open by default.

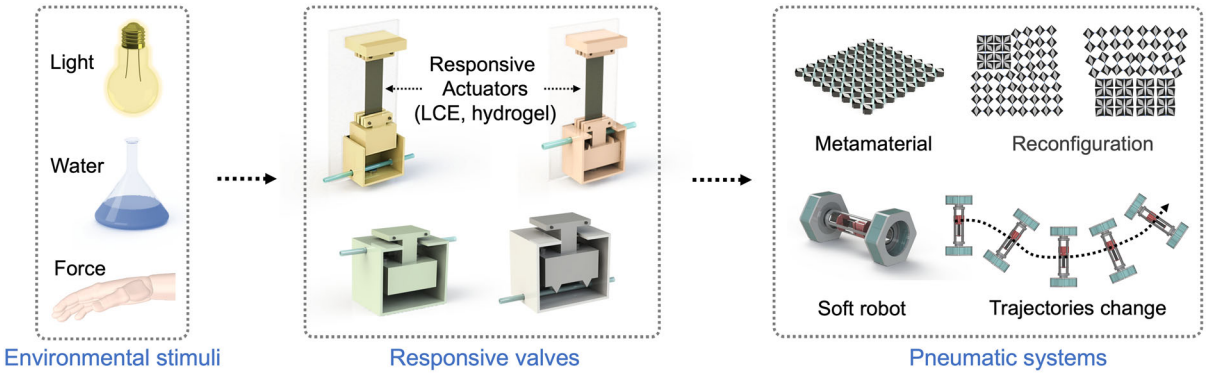

Figure 1. Overview of modular responsive valves. The responsive valves can sense and respond to environmental stimuli (light, water, and mechanical force), causing changes in a valve's state (open or closed). Multiple valves can be integrated into networks, creating responsive logic that controls the shape, properties, and/or function of metamaterial structures or soft robots.

© 2024 The Author(s). Advanced Intelligent Systems published by Wiley-VCH GmbH

26404567, 0, Downloaded from https://advanced.onlinelibrary.wiley.com/doi/10.1002/aisy.202400659, Wiley Online Library on [23/04/2025]. See the Terms and Conditions (https://onlinelibrary.wiley.com/terms-and-conditions) on Wiley Online Library for rules of use; OA articles are governed by the applicable Creative Commons License

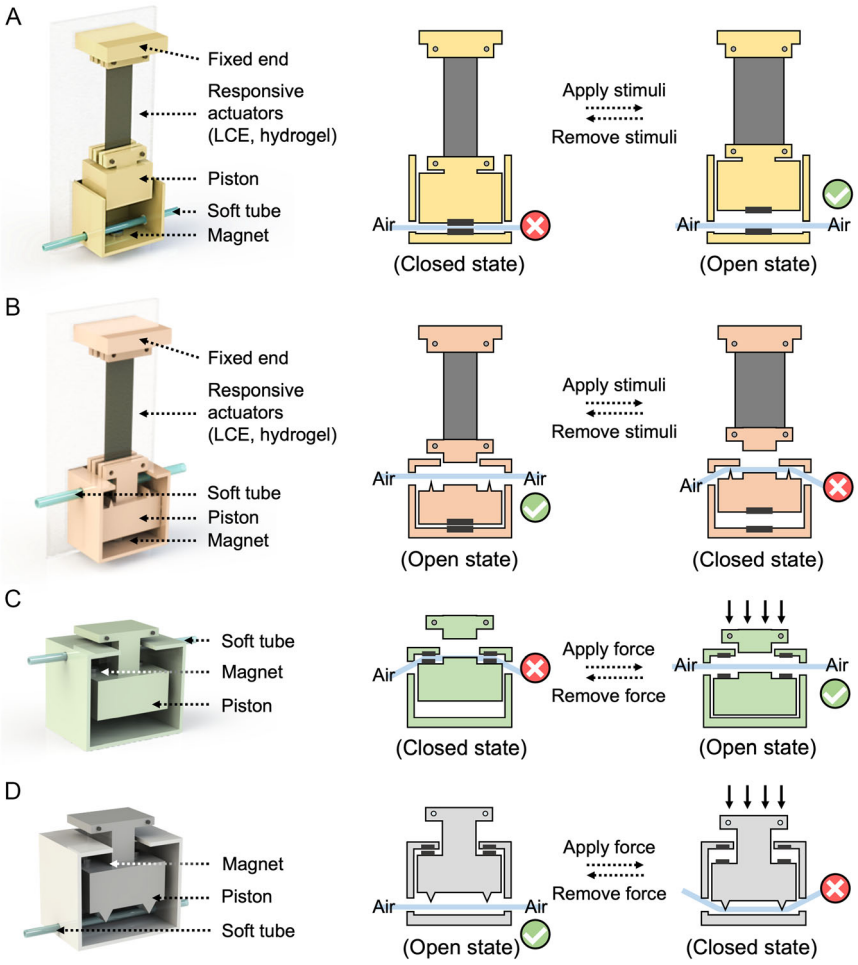

Figure 2. Design, construction, and operating principle of responsive valves. The responsive valves comprise responsive materials (LCE, hydrogel), a piston, a soft tube, and a pair of magnets. A) In this example, the valve is closed by default, with the soft tube compressed by the piston due to the attraction of magnets. Application of stimuli (light, water) to the valve results in the contraction of the responsive materials (LCE, hydrogel) thereby lifting the piston, which, in turn, opens the valve. Removal of the stimuli (inputs) results in the return of the valve to its default closed state. B) In this example, the valve is open by default. It closes when relevant external stimuli are introduced as inputs. C) In this example, the valve is closed by default. It opens when subjected to a mechanical force. D) In this example, the valve is open by default. It closes when subjected to a mechanical force. For all these examples, the valves recover their initial (default) state after the removal of the stimuli.

As shown in Figure 3B, we first characterized the light-responsive valve, which is closed by default. When light is applied to the valve, it takes ≈5 s for the valve to open. The pneumatic actuator was inflated and deflated following a sine pressure wave (see P_2 in Figure 3B). After the light was switched off, the pressure in the actuator became constant after ≈5 s (returning to its default closed state). Similarly, the light-responsive valve, which has an open state by default, was also characterized, as shown in Figure 3C. One critical parameter influencing the behavior of the valves is the strength of the magnets within the valve. The attractive force determines the critical conditions for transitioning between different states. To quantitatively characterize this effect, we designed and tested a set of responsive valve magnets with various sizes and strengths, as shown in Figure S4, Supporting Information. The valve with low-strength magnets (see valve 1 in Figure S4, Supporting Information) cannot maintain its initial closed state because of its low critical transition force. Increasing the critical transition force from 3.54 to 8.66 N, the valve's actuation time increases from 2 to 5 s. However, once the critical transition force exceeds the threshold (valve 4 with 14.08 N), the valve remains permanently closed as the force generated by the CNT-LCE cannot overcome the magnetic attraction force (Figure S4B, Supporting Information). The maximum forces generated by the CNT-LCE strip and hydrogel actuator are presented in Figure S2D,H, Supporting Information, respectively.

In addition, we submerged the water-responsive valve in water to quantify the response time of the valve. As shown in Figure 3D,E, due to the slow diffusion of water into the hydrogel, it takes 30 min (default closed) and 40 min (default open) for these responsive valves to switch their states, respectively. The recovery time for the valve to reach its initial state after swelling takes longer, as shown in Figure 3D,E. The water-responsive valve (default closed in Figure 3D and default open in

© 2024 The Author(s). Advanced Intelligent Systems published by Wiley-VCH GmbH

26404567, 0, Downloaded from https://advanced.onlinelibrary.wiley.com/doi/10.1002/aisy.202400659, Wiley Online Library on [23/04/2025]. See the Terms and Conditions (https://onlinelibrary.wiley.com/terms-and-conditions) on Wiley Online Library for rules of use; OA articles are governed by the applicable Creative Commons License

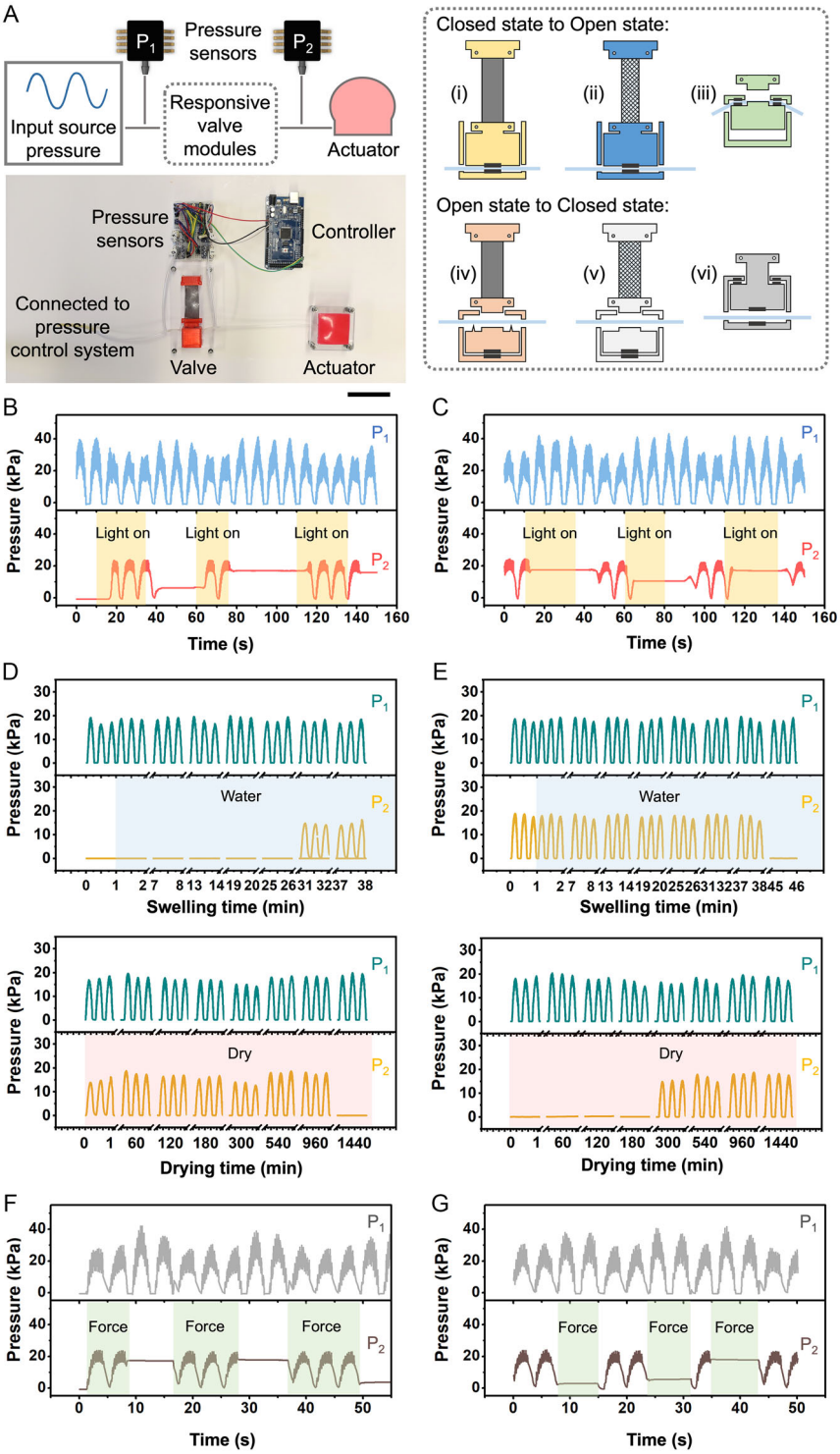

Figure 3. Characterization of responsive valves. A) Schematic and photograph of the apparatus for experimental characterization. The pressure input is a sine wave generated by a fluid control system. Multiple valve modules are placed between the fluid control system and the pneumatic actuator. The source pressure and pressure of the actuator are measured simultaneously when the external stimuli are applied. B) The response of the light-responsive valve (default closed). In this case, it takes ≈5 s for the valve to open after the light is applied. There is a similar delay for the valve to close after the light is removed. C) The response of the light-responsive valve (default open). D) The response of the water-responsive valve (default closed). The valve is first submerged in water. The valve opens ≈30 min later. Once removed from the water, the valve closes (its default state) after ≈16 h. E) The response of the water-responsive valve (default open). F) The response of the force-responsive valve (default closed). The states of the valve change immediately upon application of a sufficiently large force. G) The response of the force-responsive valve (default open). Scale bar in (A): 5 cm.

© 2024 The Author(s). Advanced Intelligent Systems published by Wiley-VCH GmbH

26404567, 0, Downloaded from https://advanced.onlinelibrary.wiley.com/doi/10.1002/aisy.202400659, Wiley Online Library on [23/04/2025]. See the Terms and Conditions (https://onlinelibrary.wiley.com/terms-and-conditions) on Wiley Online Library for rules of use; OA articles are governed by the applicable Creative Commons License

Figure 3E) recovers to their initial states after 16 and 5 h, respectively. The response of the hydrogels is slow because it is regulated by diffusion. To overcome this challenge, different approaches have been adopted, such as reducing its physical size and introducing porous features.[37] It is also worth noting that the responsive materials are not, in principle, limited to the specific materials used in this work (e.g., hydrogels or LCEs). A variety of materials with appropriate designs, such as SMPs and magnetic soft materials, could, in principle, be integrated into the valves to achieve autonomous responses in the presence of designated stimuli (e.g., temperature and magnetic fields).

To verify the repeatability and robustness of the responsive valves, we conducted cyclic tests, as shown in Figure S5 and S6, Supporting Information. The light-responsive valve demonstrated stable performance even after 30 cycles. However, the performance of the water-responsive valve degraded after three cycles, which is caused by hydrogel breakage.

Finally, the characterization of the force-responsive valves is shown in Figure 3F,G. For these valves, instead of relying on the responsive materials to interact with light or water, mechanical forces can directly trigger the translational movements of the piston. As a result, these valves instantaneously switch their states once the force is applied.

2.3. Responsive Logic Gates via Modular Valves

As demonstrated above, one type of valve module regulates the airflow based on a single, specific stimulus as an input. Some engineering applications, however, might necessitate that the pneumatic system makes decisions on multiple physical inputs from the environment. By combining different types of responsive valves, fundamental logical evaluations and more complex operations can be carried out based on the aggregate effect. This could be used, for example, to require multiple stimuli to be introduced and/or sequenced before an action is performed.

To demonstrate this behavior, we constructed logic gates with multiple stimuli-responsive valves. In **Figure 4**, we show five basic gates: "AND," "NAND," "OR," "NOR," and "XNOR." In these particular examples, we constructed the gates to make irreversible state changes due to the very different time scales of the responsive materials (e.g., CNT-LCEs and hydrogels in Figure 3). For irreversible valves, once a state change occurs, i.e., due to a relevant stimulus in the environment, the state change will remain even when the stimulus is removed. Though here we only use this effect as a practical way to bridge the different time scales of the responsive materials being fed into the logic gate, such gates may have other uses. For example, irreversible valves could be used to store discrete information without continuous energy input from the environment, taking advantage of their multistable nature, or used to produce tamper-proof soft robots.

As shown in the schematics of Figure 4, our logic system consists of different types of valve modules as we discussed above, a pneumatic soft actuator, and pressure sensors. The input end of the logic system was connected to an active custom fluid control system, ensuring that the air pressure never dropped to zero. A pressure sensor was used to record this source air pressure (P_{source}). The output of the logic system was connected to both the pneumatic soft actuator and a pressure sensor (P_{out}). Different environmental stimuli were then added as inputs, either light ("L") or water ("W"). Boolean values of "1" or "0" indicate whether a stimulus is or is not provided as an input, respectively. For example, for an experiment in which light is present but water is not, the environmental stimuli would be indicated as (L = 1, W = 0). To quantify the effect of the various valves, we define the output normalized pressure $P_{\text{normalized}} \equiv P_{\text{out}}/P_{\text{source}}$. The values "0" and "1" indicate the valve is closed or open, respectively.

As examples, Figure 4A shows an "AND" response. To achieve this function, a light-responsive valve (default closed) and a water-responsive valve (default closed) were arranged in series. Thus, the valve will only open ($P_{\text{normalized}} = 1$) when both light and water are applied to the system (L = 1 and W = 1). Figure 4B shows an arrangement with a "NAND" response. This was achieved by arranging a light-responsive valve (default open) and a water-responsive valve (default open) in parallel. With L = 1 and W = 1, both valve modules change from initially open states to closed states, blocking the passage of the air through the logic system (giving $P_{\text{normalized}} = 0$). Figure 4C shows an arrangement with an "OR" response. To achieve this, two modular valves (default closed) were arranged in parallel. When one or both valves are triggered by environmental stimuli (L = 1 or W = 1), the output is $P_{\text{normalized}} = 1$ (the logic system is open). If neither stimuli is present (L = 0 and W = 0), the output is $P_{\text{normalized}} = 0$ (the logic system is closed). Similarly, a "NOR" gate can be realized as shown in Figure 4D. Finally, we used four responsive valves to construct an "XNOR" gate. Two light-responsive valves (one default open and one default closed) and two water-responsive valves (one default open and one default closed) were divided into two groups. As shown in Figure 4E, the output $P_{\text{normalized}} = 1$ (the logic system is open) is realized when the inputs are L = W; otherwise, the output is $P_{\text{normalized}} = 0$ (the logic system is closed).

In addition to logic gates that respond to light and water, we also have constructed logic gates that respond to light and force, by simply replacing the water-responsive valve modules with force-responsive valve modules (Figure S7, Supporting Information). In principle, other stimuli-responsive materials could enable these valves to respond to a variety of additional stimuli (e.g., pH,[38] voltage,[39] magnetic field,[29,30] and so on)

2.4. Modular Responsive Pneumatic Fluid Networks

In traditional digital electronics, logic gates can be combined to implement more complicated functions. Our design can realize more complex mechanical computing by integrating modular responsive valves and corresponding logic gates in circuit-like designs, as shown in **Figure 5**A. The system includes a constant air pressure source and four independent pressure outputs. Fifteen valve modules are employed to construct pneumatic systems that regulate pressure based on environmental inputs. The final output is the result of a computational event that can include multiple complex events in the network. The four output channels of the pneumatic network connect to a pneumatic kirigami, which is a type of mechanical metamaterial with tunable shape configuration and mechanical properties. As shown in Figure 5B,

© 2024 The Author(s). Advanced Intelligent Systems published by Wiley-VCH GmbH

26404567, 0, Downloaded from https://advanced.onlinelibrary.wiley.com/doi/10.1002/aisy.202400659, Wiley Online Library on [23/04/2025]. See the Terms and Conditions (https://onlinelibrary.wiley.com/terms-and-conditions) on Wiley Online Library for rules of use; OA articles are governed by the applicable Creative Commons License

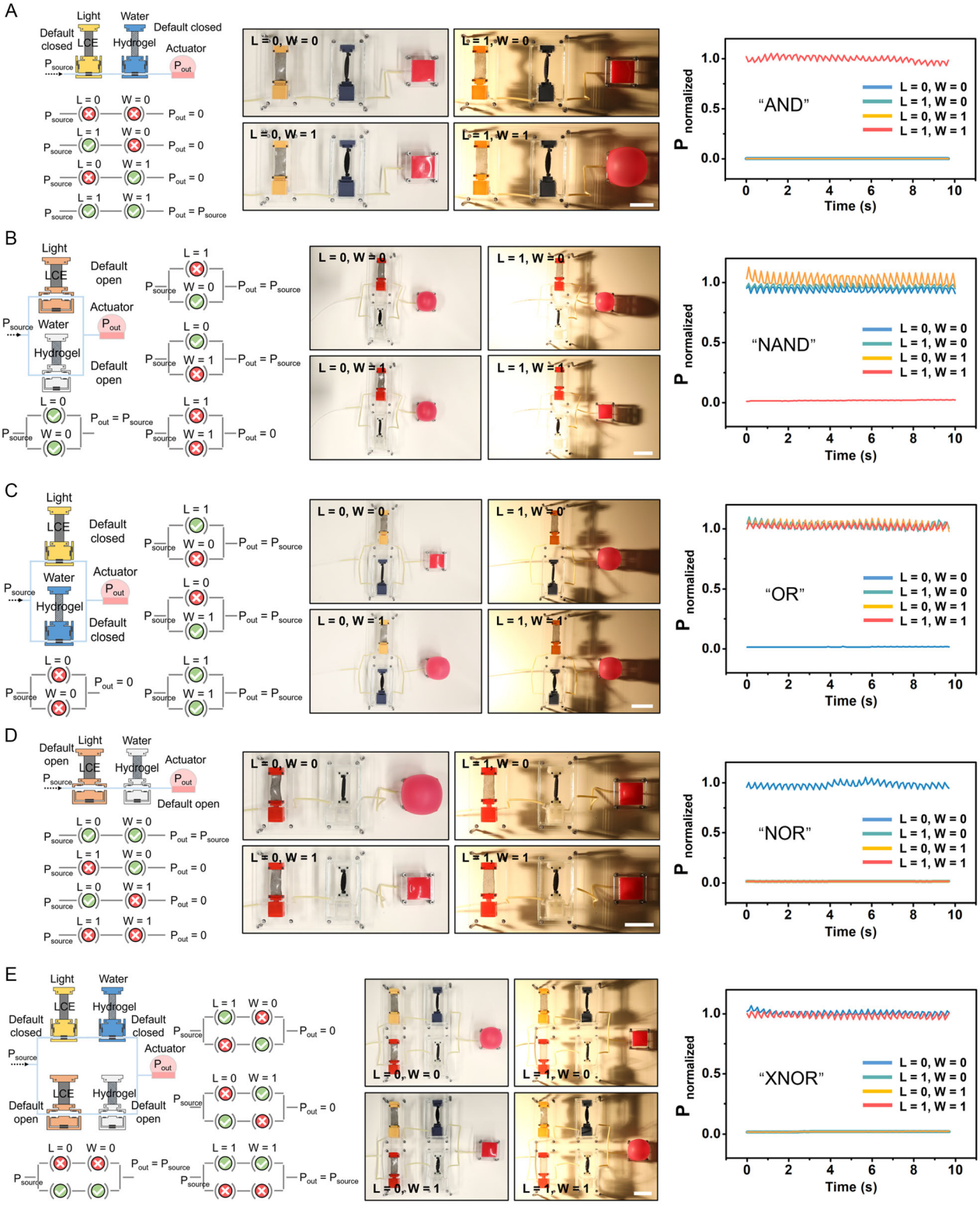

Figure 4. Logic gates based on responsive valve modules. Schematics, experimental images, and pressure measurements of A) an AND gate, B) a NAND gate, C) an OR gate, D) a NOR gate, and E) an XNOR gate. The inputs are environmental stimuli (L = light, W = water), and the outputs are the normalized pressure $P_{normalized}$ (P_{out}/P_{source}) under different conditions. Experimentally, we wait for enough time until all the valves reach the equilibrium state. All scale bars indicate 5 cm.

© 2024 The Author(s). Advanced Intelligent Systems published by Wiley-VCH GmbH

26404567, 0, Downloaded from https://advanced.onlinelibrary.wiley.com/doi/10.1002/aisy.202400659, Wiley Online Library on [23/04/2025]. See the Terms and Conditions (https://onlinelibrary.wiley.com/terms-and-conditions) on Wiley Online Library for rules of use; OA articles are governed by the applicable Creative Commons License

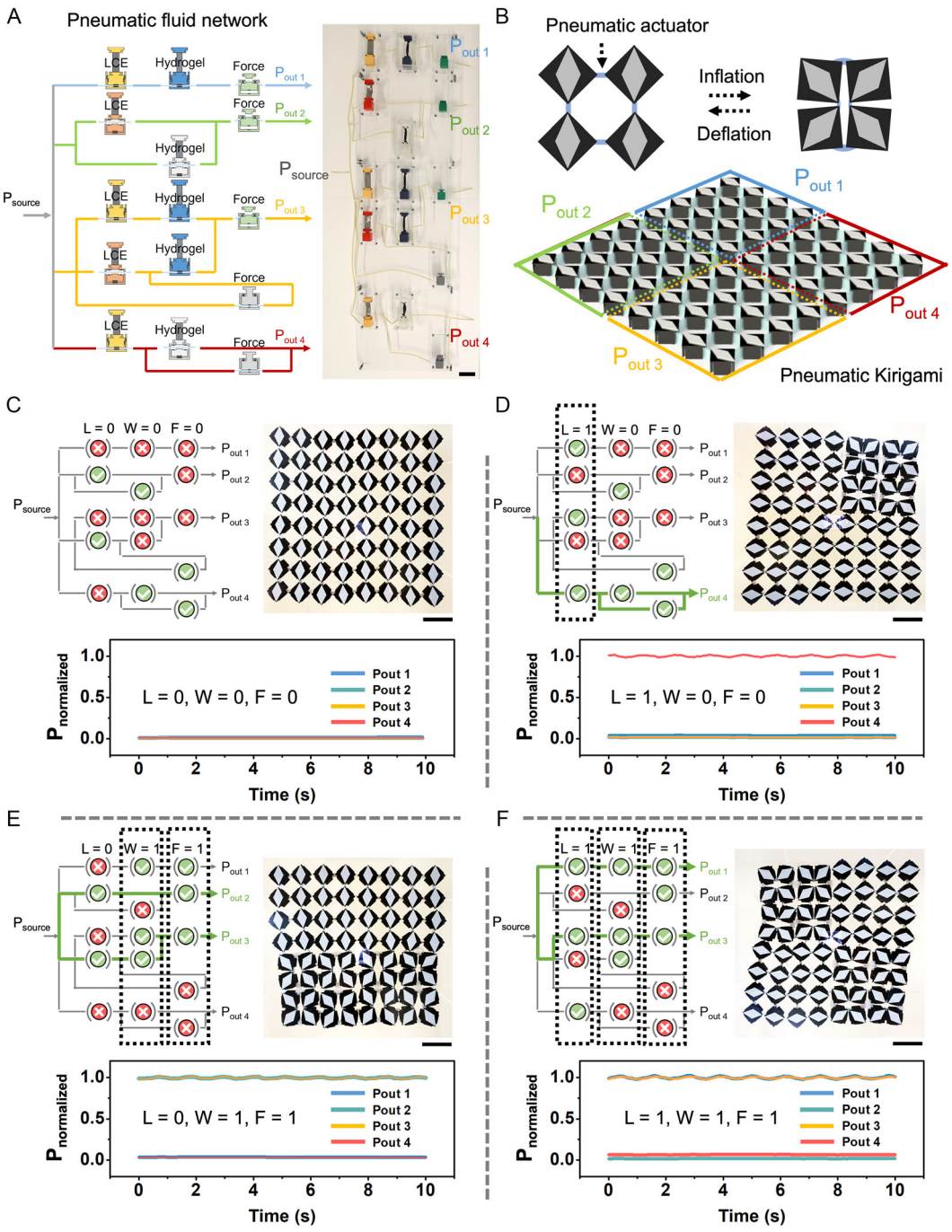

Figure 5. Pneumatic fluid networks and pneumatic kirigami with responsive valves. A) Schematic and experimental image of a pneumatic fluid network consisting of multiple types of responsive valves. The output pressures (four channels) are determined by the inputs from external stimuli (light, water, and force). B) Four output channels of the fluid network are connected to four separate domains of pneumatic kirigami. The square units of each domain can freely rotate when pressurized air is applied. C) Initially, the pressure outputs are all zero and all four domains exhibit open kirigami configurations. D) As one example, once light is applied, the pressurized air can pass through the fourth channel, triggering the kirigami to close at the top right. The morphology of the pneumatic kirigami can be changed under different stimuli as shown in E) (with water and force) and F) (with light, water, and force). Scale bar in (A): 5 cm; scale bars in (C–F): 5 cm.

this kirigami has four separate domains, each of which can freely rotate when bendable hinges are inflated by the pressurized air (Figure S8, Supporting Information). When the stimuli are applied to the pneumatic fluid network, four output channels may (or may not) block the pressurized air. The kirigami changes its shape accordingly. There are a total of $2^3 = 8$ combinations of

© 2024 The Author(s). Advanced Intelligent Systems published by Wiley-VCH GmbH

26404567, 0, Downloaded from https://advanced.onlinelibrary.wiley.com/doi/10.1002/aisy.202400659, Wiley Online Library on [23/04/2025]. See the Terms and Conditions (https://onlinelibrary.wiley.com/terms-and-conditions) on Wiley Online Library for rules of use; OA articles are governed by the applicable Creative Commons License

input values with three Boolean inputs. Here, we show four representative examples.

When no stimuli are applied to the pneumatic fluid network ($L = W = F = 0$), the four output channels are in the "off" state, which is also confirmed by the pressure measurements in Figure 5C. The status of the valve modules in the schematic, "on" (✓) or "off" (✗), indicates the final state of the valves when exposed to the corresponding environmental stimuli. As a result, all four parts of the kirigami are in the "open state" with the 2D pattern shown in Figure 5C. If the pneumatic fluid network is exposed only to light ($L = 1$, $W = F = 0$), five light-responsive valves are triggered (in the dashed rectangle in Figure 5D), resulting in switching of the state of the valves (either from open to closed or vice versa). Thus, the fourth channel is no longer blocked (see the green path in the schematic and pressure measurement of Figure 5D). The pressurized air passes through the fourth channel and flows into the top right domain of the kirigami, causing the square units to close. Similarly, the air flows into the kirigami via the second and third channels under the application of water and force ($L = 0$, $W = F = 1$), which leads to the closing of the bottom domains in the kirigami (Figure 5E). When all the external stimuli are applied to the pneumatic fluid network ($L = W = F = 1$), all the valve modules change their states. In Figure 5F, the top right and bottom left corners of the kirigami are triggered because of the opening of the first and third channels. Each combination of the environmental stimuli input corresponds to a unique 2D pattern, indicating the outcome of the computational result from the pneumatic fluid network.

The modular design approach of the responsive valves offers significant flexibility for achieving different behaviors with a pneumatic fluid network. By simply adding, removing, and rearranging the responsive valves, a network can realize different logic and thereby respond differently to a given set of environmental stimuli, enabling different computation strategies.

Figure S9, Supporting Information, shows an example of this, with a change to the arrangement and logic of the valves producing entirely different behaviors under the same environmental conditions (see Figure 5C–F and S9B–E, Supporting Information). We also note that additional degrees of freedom can be added to the pneumatic fluid network, increasing the physical intelligence of the network and potentially increasing the number of environmental stimuli that can be sensed.

2.5. Application of Responsive Valves to Pneumatic Soft Robots

To further demonstrate the idea of stimuli-responsive valves for autonomous pneumatic logic, we built a pneumatic soft rolling robot. This pneumatic soft robot contains a light-responsive valve, a 3D-printed axle, two bearings, and two hexagonal rolling actuators (**Figure 6**A,B). The hexagonal rolling actuator contains 12 inflatable chambers that are evenly distributed Figure S10A, Supporting Information. When certain chambers are inflated, the actuator can locally bulge, causing the center of gravity of the body to shift, further causing the actuator to roll. By selectively and periodically inflating and deflating designated pneumatic chambers, the soft robot rolls forward or backward. A group of six inflatable pneumatic chambers (blue and green) are in charge of moving the robot forward while another six chambers (red and orange) enable the robot to move backward (Figure S10B, Supporting Information). Figure S10C, Supporting Information, shows the soft robot moving forward. When the robot senses light, the responsive valve is triggered (schematic in Figure 6C). The piston of the valve moves up and blocks airflow through the soft tube on the top, while the soft tube at the bottom of the chamber relaxes, allowing airflow. As a result, the other group of six chambers is connected to the air supply, resulting in backward motion (Figure S7C, Supporting Information). The motion of the robot is shown in Figure 6C. The displacement of the soft robot is shown in Figure 6D as a function of cycle number. The corresponding video is shown in Movie S1, Supporting Information.

A more complex moving strategy can be achieved by redesigning and implementing another type of responsive valve, as shown in Figure 6E. In this case, two CNT-LCE strips were integrated and distributed on each side of the valve. This valve module has three stable states. When no appreciable light is present in the environment, the two CNT-LCE strips are both relaxed, causing the piston to remain in the middle. As a result, the pressurized air flows equally into the two rolling actuators, causing the soft robot to move straightforward continuously. If the robot is illuminated from one side, e.g., the left, the CNT-LCE strip on the left contracts more than the right side, causing the piston to shift its position to the left, compressing the soft tube on the left and blocking airflow to the left wheel. As a result, only the hexagonal rolling actuator on the right is inflated, which causes the robot to steer to the left (Figure 6E). Similarly, the robot steers to the right if the light is from the right The trajectory changes are shown in Figure 6F and the corresponding video is shown in Movie S2, Supporting Information.

3. Discussion

We have designed and built simple, modular mechanical valves that can sense and respond to a variety of external stimuli (light, water, and mechanical forces). By combining different types of valves, logic systems with simple computational capabilities can be achieved including basic logic ("AND," "OR," "NAND," "NOR," and "XNOR") and more computationally complex pneumatic fluid networks. Finally, these responsive valves can be readily integrated with pneumatic systems to regulate pneumatic soft robots. The trajectories of soft rolling robots can autonomously change in response to the environment without relying on electronics for decision-making. Further, the modular strategy that was used in this work is compatible with a wide variety of responsive materials. These could, in principle, enable the pneumatic system to sense, and perform computation in response to multiple stimuli. While we used LCEs and hydrogels in this work, the same principles could potentially be extended to other smart materials such as magnetoresponsive composites, SMPs, dielectric elastomers, and so on.

One limitation of the current work is the large physical size (centimeter scale) of the responsive valves, which is constrained by our current manufacturing technique (e.g., the resolution of the 3D printers and the fabrication process

© 2024 The Author(s). Advanced Intelligent Systems published by Wiley-VCH GmbH

26404567, 0, Downloaded from https://advanced.onlinelibrary.wiley.com/doi/10.1002/aisy.202400659, Wiley Online Library on [23/04/2025]. See the Terms and Conditions (https://onlinelibrary.wiley.com/terms-and-conditions) on Wiley Online Library for rules of use; OA articles are governed by the applicable Creative Commons License

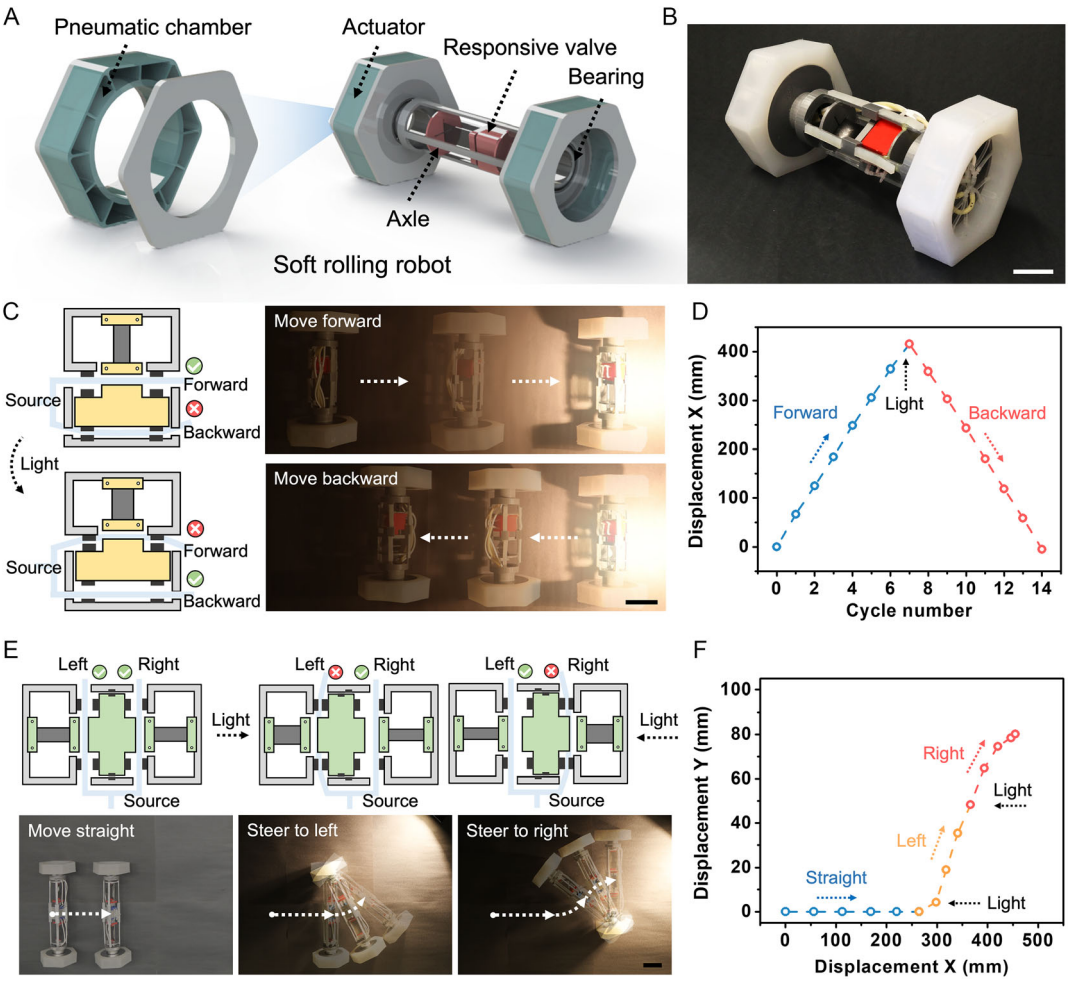

Figure 6. A rolling pneumatic robot with responsive valves. A,B) Schematic and photograph of a pneumatic soft robot, comprising two hexagonal rolling actuators (12 pneumatic chambers), two bearings, an axle, and light-responsive valves. C) The soft robot reverses its direction of motion when it encounters light in front. D) Displacement versus number of pneumatic actuation cycles of the soft robot. E) The soft robot steers under the application of light. F) The corresponding trajectory of the soft robot. Scale bars in (B, C, and E): 5 cm.

of responsive materials). However, we note that this design principle and operating mechanism could be extended to other length scales. LCEs and hydrogels can be patterned down to micrometer size via spinning.[40–42] Two photon polymerization has also demonstrated compatibility with an increasingly wide variety of materials and structures.[43] These and other approaches for reducing the size of the responsive valves could broaden the use of pneumatic soft actuators in biomedical fields (e.g., endoscopes, and stents). Another possible limitation of this work is the relatively slow response speed of hydrogels, due to slow diffusion, for both swelling and drying (Figure 3). We note, however, that these speeds would be improved by using micro-/macroporous hydrogels, which have been reported in previous work.[44] On the other hand, taking advantage of the "slow" response, the pneumatic soft robots integrated with the water-responsive valves could enable bioinspired unperceivable motion[45] or environmental regulation over long periods of time (e.g., chemical treatment).

4. Experimental Section

Materials: To fabricate CNT-LCEs, the following components were used as received, without additional modification: (1,4-bis-[4-(3-acryloyloxypropyloxy)benzoyloxy]-2-methylbenzene) (RM257, Wilshire company, 95%), 2,2′-(ethylenedioxy)diethanethiol (EDDET, Sigma–Aldrich, 95%), pentaerythritol tetrakis(3-mercapto-propionate) (PETMP, Sigma–Aldrich, 95%), dipropylamine (DPA, Sigma–Aldrich, 98%), (2-hydroxyethoxy)-2-methylpropiophenone (HHMP, Sigma–Aldrich, 95%), multiwall CNTs (MWCNTs, Sigma–Aldrich, 98%), and toluene. Hydrogel actuators were assembled from hydrogel beads (Hicarer store) and woven braided mesh tubes, without modification. The pneumatic kirigami and pneumatic soft actuators were molded from Ecoflex 30 (Smooth-On, Inc.) and Dragonskin 10 (Smooth-On, Inc.) without further modification.

Synthesis of CNT-LCE: We first prepared loosely crosslinked CNT-LCEs based on our previous study.[31] Liquid crystal (RM 257, 10 g), CNTs (MWCNT, 0.02 g), and photoinitiator (HHMP, 0.078 g) were dissolved in toluene (3.1 g). The mixture was placed in an oven at 85 °C for 30 min. Then, the spacer (EDDET, 1.9 g), tetra-arm thiol crosslinker (PETMP, 1.52 g), and catalyst (DPA, 0.032 g) were added to the mixture. After that, the mixture was stirred and degassed in the vacuum chamber.

© 2024 The Author(s). Advanced Intelligent Systems published by Wiley-VCH GmbH

26404567, 0, Downloaded from https://advanced.onlinelibrary.wiley.com/doi/10.1002/aisy.202400659, Wiley Online Library on [23/04/2025]. See the Terms and Conditions (https://onlinelibrary.wiley.com/terms-and-conditions) on Wiley Online Library for rules of use; OA articles are governed by the applicable Creative Commons License

Next, the mixture was poured into a rectangular mold ($30 \times 25 \times 0.5$ mm) for subsequent chemical reaction. Finally, we removed the sample from the mold and placed it in an oven at 85 °C for 24 h to evaporate the toluene. This procedure produces a loosely crosslinked CNT-LCE (polydomain state) strip.

Next, we applied a prestretch ($\lambda = 2$) to the loosely crosslinked CNT-LCE strip to align the liquid crystal mesogens, putting the CNT-LCE in a monodomain state. Then, the sample was exposed to UV irradiation for 1 h as a second crosslinking step. Finally, we cut the CNT-LCE strip into the dimensions $50 \times 20 \times 0.35$ mm. The characterization of the LCE is shown in Figure S2A–C, Supporting Information.

Preparation of Hydrogel Actuator: The woven braided mesh tube (constraining layer) was cut into small dimensions ($\phi 5 \times 50$ mm). Then, 0.25 g hydrogel beads were put into the tube. Finally, the ends of the tube were tightened using a zip tie and sealed with epoxy, respectively. The characterization of the hydrogel actuator is shown in Figure S2D–F, Supporting Information.

Fabrication of Responsive Valves: The responsive valves (Figure 2 and S1, Supporting Information) were constructed from 3D printed parts made from polylactic acid, silicone tubes, magnets, and responsive materials (hydrogels, CNT-LCEs). The 3D-printed parts were designed in Solidworks and printed using a commercial 3D printer (MakerGear M3). We then assembled each valve as shown in Figure S1, Supporting Information. In all cases, the ends of the responsive materials were attached to the 3D-printed connectors using epoxy. The connectors on both sides were attached via screws to the fixed end on the top and the piston on the bottom, making it easy to change materials.

Fluid Control System and Pressure Measurements: We constructed a custom fluid control system to allow control of the pressures used in the experiments. This system includes a microcontroller (Arduino Mega), solenoid valves and manifold, air pump, pressure sensors (Adafruit MPRLS), and MOSFET (metal–oxide–semiconductor field-effect transistor). Pressurized air can be produced by the pump, regulated by the solenoid valves via PWM, and measured by the pressure sensors. The measured pressure can be recorded with the Arduino IDE using Python scripts.

Fabrication of Pneumatic Kirigami: The fabrication of the pneumatic kirigami is shown in Figure S5, Supporting Information. The PneuNet bending actuators and passive connections were molded using 3D-printed molds and Dragonskin 10 (Smooth-On, Inc.). The 3D-printed squares with white arrows were inserted into the connection points to form the 2D pneumatic kirigami. The arrows were used to indicate the rotation of the kirigami squares. Air tubes were inserted into each pneumatic bending actuator and connected to the external pressure source.

Fabrication of Hexagonal Rolling Actuator: The hexagonal rolling actuator was constructed following a previous study.[46] As above, we 3D-printed molds. The uncured silicone precursor (Dragonskin 10) was poured into the molds and cured. After 24 h, the cured silicones were removed. The top and bottom parts were glued together using uncured silicone. Finally, we inserted tube fittings (McMaster-Carr) and sealed them using Sil-poxy (Smooth-On, Inc.). The tube fittings were connected to the external fluid control system.

Supporting Information

Supporting Information is available from the Wiley Online Library or from the author.

Acknowledgements

The authors gratefully acknowledge support via AFOSR award numbers FA9550-23-1-0416 and FA9550-23-1-0299 and NSF award numbers 2239308 and 2041410.

Conflict of Interest

The authors declare no conflict of interest.

Author Contributions

Qiguang He: Conceptualization (equal); Data curation (equal); Formal analysis (equal); Investigation (equal); Methodology (equal); Writing—original draft (equal); Writing—review & editing (equal). **Rui Yin**: Conceptualization (equal); Data curation (equal); Formal analysis (equal); Investigation (equal); Methodology (equal); Writing—original draft (equal); Writing—review & editing (equal). **Yucong Hua**: Conceptualization (equal); Data curation (equal); Formal analysis (equal); Investigation (equal); Methodology (equal); Writing—original draft (equal); Writing—review & editing (equal). **Hang Shu**: Investigation (supporting). **Xiaoheng Zhu**: Investigation (supporting). **A. B. M. Tahidul Haque**: Investigation (supporting); Writing—review & editing (supporting). **Samuele Ferracin**: Investigation (supporting); Writing—review & editing (supporting). **Saheli Patel**: Writing—review & editing (supporting). **Weijian Jiao**: Investigation (supporting). **Jordan R. Raney**: Conceptualization (equal); Formal analysis (equal); Funding acquisition (lead); Investigation (equal); Methodology (equal); Project administration (lead); Resources (lead); Supervision (lead); Writing—original draft (supporting); Writing—review & editing (equal). **Qiguang He**, **Rui Yin**, and **Yucong Hua** contributed equally to this work.

Data Availability Statement

The data that support the findings of this study are available in the supplementary material of this article.

Keywords

autonomy, liquid crystal elastomers, physical intelligence, soft robots, stimuli-responsive materials

Received: August 3, 2024
Revised: October 22, 2024
Published online:

[1] E. Brown, N. Rodenberg, J. Amend, A. Mozeika, E. Steltz, M. R. Zakin, H. Lipson, H. M. Jaeger, *Proc. Natl. Acad. Sci.* **2010**, *107*, 18809.
[2] K. H. L. Heung, Z. Q. Tang, L. Ho, M. Tung, Z. Li, R. K. Y. Tong, in *2019 IEEE 16th Int. Conf. Rehabilitation Robotics (ICORR)*, IEEE, Piscataway, NJ **2019**, pp. 65–70.
[3] J. Zou, M. Feng, N. Ding, P. Yan, H. Xu, D. Yang, N. X. Fang, G. Gu, X. Zhu, *Natl. Sci. Rev.* **2021**, *8*, nwab048.
[4] M. T. Tolley, R. F. Shepherd, B. Mosadegh, K. C. Galloway, M. Wehner, M. Karpelson, R. J. Wood, G. M. Whitesides, *Soft Rob.* **2014**, *1*, 213.
[5] B. Mosadegh, P. Polygerinos, C. Keplinger, S. Wennstedt, R. F. Shepherd, U. Gupta, J. Shim, K. Bertoldi, C. J. Walsh, G. M. Whitesides, *Adv. Funct. Mater.* **2014**, *24*, 2163.
[6] R. F. Shepherd, F. Ilievski, W. Choi, S. A. Morin, A. A. Stokes, A. D. Mazzeo, X. Chen, M. Wang, G. M. Whitesides, *Proc. Natl. Acad. Sci.* **2011**, *108*, 20400.
[7] F. Ilievski, A. D. Mazzeo, R. F. Shepherd, X. Chen, G. M. Whitesides, *Angew. Chem.* **2011**, *123*, 1930.
[8] D. Drotman, M. Ishida, S. Jadhav, M. T. Tolley, *IEEE/ASME Trans. Mechatron.* **2018**, *24*, 78.
[9] Y. Tang, Q. Zhang, G. Lin, J. Yin, *Soft Rob.* **2018**, *5*, 592.

© 2024 The Author(s). Advanced Intelligent Systems published by Wiley-VCH GmbH

26404567, 0, Downloaded from https://advanced.onlinelibrary.wiley.com/doi/10.1002/aisy.202400659, Wiley Online Library on [23/04/2025]. See the Terms and Conditions (https://onlinelibrary.wiley.com/terms-and-conditions) on Wiley Online Library for rules of use; OA articles are governed by the applicable Creative Commons License

[10] H. K. Yap, J. H. Lim, F. Nasrallah, J. C. H. Goh, R. C. H. Yeow, in *2015 IEEE Int. Conf. Robotics and Automation (ICRA)*, IEEE, Piscataway, NJ **2015**, pp. 4967–4972.
[11] G. Gu, N. Zhang, H. Xu, S. Lin, Y. Yu, G. Chai, L. Ge, H. Yang, Q. Shao, X. Sheng, X. Zhu, *Nat. Biomed. Eng.* **2021**, *7*, 589.
[12] R. A. Shveda, A. Rajappan, T. F. Yap, Z. Liu, M. D. Bell, B. Jumet, V. Sanchez, D. J. Preston, *Sci. Adv.* **2022**, *8*, eabo2418.
[13] Z. Xie, F. Yuan, J. Liu, L. Tian, B. Chen, Z. Fu, S. Mao, T. Jin, Y. Wang, X. He, G. Wang, *Sci. Rob.* **2023**, *8*, eadh7852.
[14] J. H. Pikul, S. Li, H. Bai, R. T. Hanlon, I. Cohen, R. F. Shepherd, *Science* **2017**, *358*, 210.
[15] Y. Chi, Y. Hong, Y. Zhao, J. Yin, *Sci. Adv.* **2022**, *8*, eadd3788.
[16] N. Farrow, N. Correll, in *2015 IEEE/RSJ Int. Conf. Intelligent Robots and Systems (IROS)*, IEEE, Piscataway, NJ **2015**, pp. 2317–2323.
[17] T. Yamaguchi, T. Kashiwagi, T. Arie, S. Akita, K. Takei, *Adv. Intell. Syst.* **2019**, *1*, 1900018.
[18] W. Liu, Y. Duo, J. Liu, F. Yuan, L. Li, L. Li, G. Wang, B. Chen, S. Wang, H. Yang, Y. Liu, Y. Mo, Y. Wang, B. Fang, F. Sun, X. Ding, C. Zhang, L. Wen, *Nat. Commun.* **2022**, *13*, 5030.
[19] H. Yasuda, P. R. Buskohl, A. Gillman, T. D. Murphey, S. Stepney, R. A. Vaia, J. R. Raney, *Nature* **2021**, *598*, 39.
[20] M. Sitti, *Extreme Mech. Lett.* **2021**, *46*, 101340.
[21] Q. He, S. Ferracin, J. R. Raney, *Nat. Comput. Sci.* **2024**, *4*, 567.
[22] P. Rothemund, A. Ainla, L. Belding, D. J. Preston, S. Kurihara, Z. Suo, G. M. Whitesides, *Sci. Rob.* **2018**, *3*, eaar7986.
[23] D. J. Preston, P. Rothemund, H. J. Jiang, M. P. Nemitz, J. Rawson, Z. Suo, G. M. Whitesides, *Proc. Natl. Acad. Sci.* **2019**, *116*, 7750.
[24] D. Drotman, S. Jadhav, D. Sharp, C. Chan, M. T. Tolley, *Sci. Rob.* **2021**, *6*, eaay2627.
[25] O. D. Yirmibeşoğlu, T. Oshiro, G. Olson, C. Palmer, Y. Mengüç, *Front. Rob. AI* **2019**, *6*, 40.
[26] M. Warner, E. M. Terentjev, *Liquid Crystal Elastomers*, Vol. *120*, Oxford University Press, Oxford, UK **2007**.
[27] M. Behl, A. Lendlein, *Mater. Today* **2007**, *10*, 20.
[28] L. Ionov, *Mater. Today* **2014**, *17*, 494.
[29] Y. Kim, H. Yuk, R. Zhao, S. A. Chester, X. Zhao, *Nature* **2018**, *558*, 274.
[30] W. Hu, G. Z. Lum, M. Mastrangeli, M. Sitti, *Nature* **2018**, *554*, 81.
[31] Q. He, R. Yin, Y. Hua, W. Jiao, C. Mo, H. Shu, J. R. Raney, *Sci. Adv.* **2023**, *9*, eade9247.
[32] Z. Wang, K. Li, Q. He, S. Cai, *Adv. Mater.* **2019**, *31*, 1806849.
[33] C. Ahn, X. Liang, S. Cai, *Adv. Mater. Technol.* **2019**, *4*, 1900185.
[34] Y. Wang, A. Dang, Z. Zhang, R. Yin, Y. Gao, L. Feng, S. Yang, *Adv. Mater.* **2020**, *32*, 2004270.
[35] Y. Wang, R. Yin, L. Jin, M. Liu, Y. Gao, J. Raney, S. Yang, *Adv. Funct. Mater.* **2023**, *33*, 2210614.
[36] H. Na, Y.-W. Kang, C. S. Park, S. Jung, H.-Y. Kim, J.-Y. Sun, *Science* **2022**, *376*, 301.
[37] Y. Zhong, L. Zhang, X. Li, B. E. Fil, C. D. Daz-Marn, A. C. Li, X. Liu, A. LaPotin, E. N. Wang, *Nat. Rev. Mater.* **2024**, *9*, 681.
[38] C. Yang, F. Su, Y. Xu, Y. Ma, L. Tang, N. Zhou, E. Liang, G. Wang, J. Tang, *ACS Macro Lett.* **2022**, *11*, 347.
[39] Y. Guo, Q. Qin, Z. Han, R. Plamthottam, M. Possinger, Q. Pei, *SmartMat* **2023**, *4*, e1203.
[40] Q. He, Z. Wang, Y. Wang, Z. Wang, C. Li, R. Annapooranan, J. Zeng, R. Chen, S. Cai, *Sci. Rob.* **2021**, *6*, eabi9704.
[41] W. Hou, J. Wang, J. Lv, *Adv. Mater.* **2023**, *35*, 2211800.
[42] X. Wei, Q. Wu, L. Chen, Y. Sun, L. Chen, C. Zhang, S. Li, C. Ma, S. Jiang, *ACS Appl. Mater. Interfaces* **2023**, *15*, 10030.
[43] M. Zhang, H. Shahsavan, Y. Guo, A. Pena-Francesch, Y. Zhang, M. Sitti, *Adv. Mater.* **2021**, *33*, 2008605.
[44] B. Sun, Z. Wang, Q. He, W. Fan, S. Cai, *Soft Matter* **2017**, *13*, 6852.
[45] F. Zhang, M. Yang, X. Xu, X. Liu, H. Liu, L. Jiang, S. Wang, *Nat. Mater.* **2022**, *21*, 1357.
[46] L. Jin, A. E. Forte, K. Bertoldi, *Adv. Sci.* **2021**, *8*, 2101941.

© 2024 The Author(s). Advanced Intelligent Systems published by Wiley-VCH GmbH

26404567, 0, Downloaded from https://advanced.onlinelibrary.wiley.com/doi/10.1002/aisy.202400659, Wiley Online Library on [23/04/2025]. See the Terms and Conditions (https://onlinelibrary.wiley.com/terms-and-conditions) on Wiley Online Library for rules of use; OA articles are governed by the applicable Creative Commons License